ISSN 0029-3865

CNPq

CBPF – CENTRO BRASILEIRO DE PESQUISAS FÍSICAS

Notas de Física

CBPF-NF-058/93

Capillary Wave Approach to Order-Order Fluid Interfaces in the 3D Three-State Potts Model

by

Paolo Provero and Stefano Vinti

Rio de Janeiro
1993

ISSN 0029-3865

CBPF-NF-058/93

Capillary Wave Approach to Order-Order Fluid Interfaces in the 3D Three-State Potts Model

by

Paolo Provero and Stefano Vinti*†

†Centro Brasileiro de Pesquisas Físicas — CBPF/CNPq
Rua Dr. Xavier Sigaud, 150
22290-180 – Rio de Janeiro, RJ – Brasil
and
Dipartimento di Fisica Teorica
Università di Torino
Via P. Giuria 1
10125 Torino, Italia[1]

*Theoretical Physics Institute
University of Minnesota
Minneapolis, MN 55455, USA[2]

TPI-MINN-93/46-T
DFTT 58/93 September 1993

[1]e-mail:vinti@.infn.it
[2]e-mail:paolo@physics.spa.umn.edu

CBPF-NF-058/93

Abstract

The physics of fluid interfaces between domains of different magnetization in the ordered phase of the 3D Z_3 Potts model is studied by means of a Monte Carlo simulation. The interface free energy is shown to be in agreement with the predictions of the capillary wave model, supporting the idea of the universality of this description of interfaces in 3D statistical models.

Key-words: Statistical modes; Thermal physics

It is well known that, between the critical and the roughening temperature, 3D spin systems on finite volumes show domain walls separating coexisting phases which behave as *fluid interfaces*.

The finite-size effects in the free energy of a fluid interface are dominated by long-wavelength fluctuations and a correct physical description of the critical properties of the surface cannot neglect their contributions [1].

The *capillary wave* (CW) approach [2] assumes an effective hamiltonian, proportional to the area of the surface, describing the collective degrees of freedom. It has been recently shown [3] that rather strong finite-size effects, depending on the shape of the lattice, can be described in terms of a gaussian model of CW: the predictions of the model have been tested with high accuracy in the scaling region of the 3D Ising model. It has also been pointed out that higher order corrections to the gaussian model can be taken into account, at least in principle, to verify the CW approach.

In this paper we study the finite-size scaling behaviour of fluid ordered-ordered interfaces of a different statistical system: the 3D three-state Potts model. We verify the high degree of universality of the CW description and we show that higher order contributions to the "area" effective hamiltonian cannot be ignored.

According to the CW model, the interface between two domains of different magnetization in the ordered phase of a 3D spin system, above the roughening temperature, is described by the partition function

$$Z_{cw} = \int [Dx] \exp\{-\sigma A[x]\} \quad , \tag{1}$$

where the function $x(r,t)$ describe the displacement from the equilibrium position of the interface, σ is the reduced (ordered-ordered) interface tension and $A[x]$ is the area of the interface

$$A[x] = \int_0^R dr \int_0^T dt \sqrt{1 + \left(\frac{\partial x}{\partial r}\right)^2 + \left(\frac{\partial x}{\partial t}\right)^2} \quad . \tag{2}$$

It should be mentioned that (2) coincides with the Nambu-Goto string action in $D = 3$ in a particular gauge if one neglects the longitudinal degrees of freedom, which however decouple only in $D = 26$. From this point of view (2) is not expected to be the *exact* action describing fluid interfaces but at least the dominant contribution: as we will show this is indeed the case.

To compare the predictions of the CW model with numerical results from Monte Carlo (MC) simulations, we have chosen generic $3D$ lattices

of $R \times T \times L$ sites, with $L \gg R, T$. Periodic boundary conditions are taken in each direction, the 2D field $x(r,t)$ being defined on the rectangle $(r,t) \in [0,R] \times [0,T]$ with opposite edges identified, i.e. on a torus.

The partition function (1) cannot be computed exactly, but it is possible to express it as an expansion in powers of the adimensional parameter σRT: the two-loop expansion of Z_{cw} can then be written as

$$Z_{cw}(R,T) \propto e^{-\sigma RT}\; Z_q^{(1\ loop)}\left(\frac{R}{T}\right) \cdot Z_q^{(2\ loop)}(R,T) \quad . \tag{3}$$

The 1-loop contribution (namely the gaussian approximation), obtained retaining only the quadratic term in the expansion of (2), is nothing else than the exact partition function of a 2D conformal invariant free boson on a torus of modular parameter $\tau = i\frac{R}{T}$ [4, 5, 3]

$$Z_q^{(1\ loop)}\left(\frac{R}{T}\right) = \sqrt{\frac{T}{R}}\left|\eta\left(i\frac{R}{T}\right)\right|^{-2} \quad , \tag{4}$$

while the 2-loop term can be calculated perturbatively expanding (2) at the next-to-leading order [6]

$$\begin{aligned} Z_q^{(2\ loop)}(R,T) &= 1 + \frac{1}{2\sigma RT}\left\{\left[\frac{\pi}{6}\frac{R}{T}E_2\left(i\frac{R}{T}\right)\right]^2 - \frac{\pi}{6}\frac{R}{T}E_2\left(i\frac{R}{T}\right) + \frac{3}{4}\right\} \\ &+ O\left[(\sigma RT)^{-2}\right] \quad . \end{aligned} \tag{5}$$

The two functions η and E_2 appearing above are respectively the Dedekind function and the second Eisenstein series:

$$\begin{aligned} \eta(\tau) &= q^{1/24}\prod_{n=1}^{\infty}(1-q^n), \qquad q \equiv \exp(2\pi i\tau) \\ E_2(\tau) &= 1 - 24\sum_{n=1}^{\infty}\frac{n\,q^n}{1-q^n} \quad . \end{aligned}$$

The three-state Potts model is defined by the partition function

$$Z = \sum_{\{\sigma_i\}} \exp\left\{-\beta\sum_{i,\hat{\mu}}\left[1 - Re(\sigma_i^{*}\sigma_{i+\hat{\mu}})\right]\right\} \tag{6}$$

where the variables σ_i are defined on a three–dimensional hypercubic lattice and take the values

$$\sigma_i = \exp\left(\frac{2\pi i n_i}{3}\right) \qquad n_i = 0, 1, 2 \ . \tag{7}$$

In the termodynamic limit the Potts model is known to undergo a (weak) first–order phase transition at $\beta_c = 0.36708(2)$ [7] and the roughening temperature can be estimate to be $\beta_r \sim 0.93$ [8]. For $\beta > \beta_c$ the symmetry is spontaneously broken and there are three ordered vacua, while at $\beta = \beta_c$ also the disordered vacuum coexists with the previous ones.

In the finite *cylindric* geometry we are considering spontaneous symmetry breaking at low temperature cannot occur: the degeneracy of the ground state is removed, the energy of the symmetric, Z_3 invariant, ground state being separated by an energy splitting E from the two degenerate mixed-symmetry states.

The energy splitting is due to tunneling between the vacua and is directly linked to the free energy of the interface [9]. According to the CW model, for $\beta_r > \beta > \beta_c$, we assume [1, 2, 3], $R \geq T$,

$$E(R,T) = C\, e^{-\sigma RT}\, Z_q^{(1\ loop)}\left(\frac{R}{T}\right) \cdot Z_q^{(2\ loop)}(R,T) \tag{8}$$

$$C = \frac{\delta}{Z_q^{(1\ loop)}(1)}$$

where δ is an unpredicted constant and a convenient normalization has been chosen.

We would like to stress that the 2–loop contribution (5) does not depend only on the ratio $z = R/T$, like the 1–loop term (4), but also on the minimal area $A_m = RT$. If we put $z = 1$, $A_m = R^2$, in (8) we obtain

$$E(R,R) = \delta\, e^{-\sigma R^2}\left\{1 + \frac{1}{2\sigma R^2}\left[\left(\frac{\pi}{6}f\right)^2 - \frac{\pi}{6}f + \frac{3}{4}\right]\right\} \ , \tag{9}$$

where $f \equiv E_2(i)$. The *classical* result [9]

$$E_{cl}(R) = \delta\, e^{-\sigma R^2} \tag{10}$$

can be recovered only neglecting the 2–loop contribution.

The comparison between the formula (8-10) and the computation of E from MC simulations provides a simple and stringent way to verify the CW predictions.

To extract the energy splitting E from MC-generated ensembles we follow the procedure of [10]. Defining the time-slice magnetization

$$S_k \equiv \frac{1}{RT} \sum_{x_1=1}^{R} \sum_{x_2=1}^{T} \sigma(x_1, x_2, k) \quad , \tag{11}$$

where $k = 0, 1, \ldots, \frac{L}{2}$, we compute the correlation function

$$G(k) \equiv \langle S_0 S_k^* \rangle \tag{12}$$

and we extract the transfer matrix low energy levels from the asymptotic k-dependence of $G(k)$

$$\begin{aligned} G(k) \cdot Z &= c_0 \{\exp(-kE) + \exp[-(L-k)E]\} \\ &\quad + c_1 \{\exp(-kE') + \exp[-(L-k)E']\} + \ldots \qquad (13) \\ Z &= 1 + 2e^{-LE} + \ldots \qquad (14) \end{aligned}$$

$Z \equiv \mathrm{tr}\ e^{-LH}$ being the partition function (the next-to-leading energy level E' turns out to be non-negligible in our range of parameters).
Having so extracted the energy splitting E from the MC data for different values of the lattice sizes, we can compute the ordered-ordered interface tension σ and the constant δ by fitting our data with the formula (8).

We have performed our simulations at $\beta = 0.3680$, the longest lattice size was fixed at $L = 120$, the other sizes varied in the range $9 \leq T \leq 11$, $10 \leq R \leq 36$, $(R \geq T)$. This value of β is enough inside the ordered phase to make highly suppressed the probability of formation of ordered-disordered interfaces [11] but presents a correlation length large enough to make the lattice artifacts negligible and to consider domain walls as fluid interfaces.

The fact that the disordered phase is substantially absent at this β can be seen from the hystograms of the real part of the magnetization [12]

$$ReM \equiv Re\left(\frac{1}{L}\sum_{k=1}^{L} S_k\right) \tag{15}$$

as is seen, for example, in Fig.1. The modulus of the magnetization at this β is about $0.44 - 0.50$ for the volumes we are considering: in this figure (the projection on the real axis of) the ordered vacua are clearly visible while the peak centered at $ReM = 0$, which would signal the presence of the disordered phase, is absent.

Fig. 2 represents a typical distribution of the magnetization M for a sample of our MC-generated configurations. Most of the configurations consist of a single phase or of two phases separated by two interfaces (the minimum number compatible with periodic boundary conditions). The single-phase configurations are represented by the three clusters of points corresponding to the three degenerate vacua: the two-interface configurations form the straight lines joining these clusters. Three-interface configurations, which tend to fill uniformly the interior of the triangle, are clearly visible in Fig. 3: it corresponds to a $T = 10$, $R = 20$ lattice and to a larger probability of having tunneling events (i.e. interfaces) while these are much more suppressed for the lattice of Fig. 2 ($T = R = 18$).

We have used a Swendsen-Wang cluster algorithm [13] to perform our MC simulations. To keep under control correlations in MC time and cross-correlations between the $G(k)$ observables, we have systematically scattered our measurements avoiding to measure two different observables at the same MC time. We have made from $0.6 \cdot 10^6$ to $1.8 \cdot 10^6$ sweep for each experiment, depending on the lattice sizes, obtaining about 10^3 data per observable. However, the covariance matrix turns out to be far different from the diagonal form, which one expects from a sample of statistical independent data. We have taken it into account including the covariance matrix in the fitting procedure to formula (13) to extract the energy gap E: the results are reported in Tab. 1.

Fitting our results for the energy gaps E with the CW predictions (8) we obtain the following values of the interface tension and of the constant:

$$\sigma = 0.009912(75)$$
$$\delta = 0.1377(19)$$

with a χ^2 per degree of freedom and confidence level

$$\chi^2 = 0.73 \qquad C.L. = 0.82 \tag{16}$$

thus confirming the accuracy of the CW model. In Tab. 1 the MC results for E are compared with the predictions of formula (8) in which the best-fit values of δ and σ have been substituted. This comparison is represented graphically in Fig. 4.

T	R	E (MC)	χ^2	C.L.	E (CW)
10	10	0.06399(51)	0.89	0.65	0.06399
12	12	0.03924(54)	1.07	0.36	0.03882
14	14	0.02201(54)	0.75	0.80	0.02227
16	16	0.01234(32)	0.95	0.52	0.01196
18	18	0.00508(71)	1.03	0.42	0.00598
20	20	0.00305(68)	0.95	0.57	0.00278
9	18	0.04108(73)	0.54	0.97	0.04105
9	21	0.03467(96)	0.99	0.47	0.03528
9	24	0.0293(11)	1.09	0.34	0.03082
9	27	0.0283(10)	0.90	0.61	0.02723
9	30	0.0235(11)	1.16	0.27	0.02427
9	36	0.0188(13)	0.98	0.48	0.01959
10	18	0.03127(47)	0.44	0.99	0.03119
10	20	0.02670(61)	1.01	0.45	0.02710
10	22	0.02339(34)	0.88	0.64	0.02374
10	24	0.02049(46)	0.79	0.75	0.02092
10	26	0.01960(47)	1.02	0.44	0.01854
10	28	0.01644(70)	0.83	0.69	0.01650
10	30	0.01473(88)	0.84	0.80	0.01473
11	20	0.02024(75)	1.17	0.25	0.02049
11	22	0.01766(78)	1.05	0.39	0.01735
11	24	0.01495(61)	0.77	0.77	0.01479
11	26	0.01292(69)	0.67	0.84	0.01267
11	28	0.01024(91)	0.66	0.87	0.01090
11	32	0.0078(12)	0.85	0.73	0.00815

Tab. 1. *The values of E are reported with the χ^2 per degree of freedom and the confidence levels, as obtained from the fit of $G(k)$ with formula (13). The values in the last column are obtained from the best fit of all data to formula (8). The same data are plotted in Fig. 4.*

The importance of the inclusion of the 2-loop contributions can be seen by fitting the MC data with the formula

$$E(R,T) = \delta\, e^{-\sigma RT} \tag{17}$$

and with the 1–loop approximation ($R \geq T$)

$$E(R,T) = \delta\, e^{-\sigma RT}\, \frac{Z_q^{(1\ loop)}\left(\frac{R}{T}\right)}{Z_q^{1\ loop}(1)} \quad . \tag{18}$$

In the former case we obtain $\chi^2 = 36.3$, in the latter $\chi^2 = 3.60$: the 2–loop correction must be included to obtain a good agreement with numerical data.

We have already noted that the 2–loop corrections affect the value of E also for symmetric ($T = R$) lattices (cfr. (9)), in contrast to what happens for the scale–invariant 1–loop contribution (18) [3]. Indeed, the importance of including 2–loop corrections can be seen fitting only the energy gaps E obtained on symmetric lattices ($T = R$): using the 2–loop expression (9) we obtain $\chi^2 = 0.79$, while the classical formula (17) gives $\chi^2 = 1.48$. The results of all these fits are summarized in Tab. 2.

Data	Approx.	σ	δ	χ^2	C.L.
all	2–loop	0.009912(75)	0.1377(19)	0.73	0.82
all	1–loop	0.010053(75)	0.1724(23)	3.60	0.00
all	class.	0.008092(75)	0.1395(19)	36.3	0.00
$T = R$	2–loop	0.00981(14)	0.1361(26)	0.79	0.53
$T = R$	class.	0.01075(14)	0.1866(36)	1.48	0.20
$T = 11$	2–loop	0.00997(69)	0.140(24)	0.26	0.90
$T = 11$	1–loop	0.00965(69)	0.151(26)	0.22	0.92

Tab. 2. *Results of the fit of E with 2–loop, 1–loop and classical approximations of the CW model, considering all values of (R,T), symmetric (R,R) lattices or $(R,T{=}11)$ lattices.*

We would like to stress the remarkable stability of the results obtained with the 2–loop approximation fitting all the data or only the symmetric ones. This can be seen comparing the values of σ and δ given in the first and fourth line of Tab. 2. On the other hand, the result obtained using the classical formula (17) is not compatible with the previous ones even using only the symmetric data, as it is shown in the fifth line of the same table. The best fit curve obtained from (17) in the latter case is plotted in Fig. 5 were also the "asymmetric" MC data are reported for comparison.
We would also like to observe that a good agreement with the 1–loop approximation of the CW model can be obtained [3] if one considers low values

of ratios $z = R/T$ and hight values of the minimal area $A_m = RT$, i.e. the 2-loop contribution (8) are maximally suppressed. This is show in the last two lines of Tab. 2 and in Fig.6.
Finally it should be remarked that it is crucial to take into account the CW contributions (i.e. to know the form of the finite size corrections to the fluid interfaces free energy) to be able on one side to extract correct informations on physical observable and on the other to use different lattice geometries, as it has been very recently shown [14].

In conclusion, we have shown that the CW model in the 2-loop approximation provides an excellent description of order-order interfaces in the 3D three-state Potts model. This result, together with the corresponding one for the 3D Ising model [3], strongly supports the hypothesis of the universality of the CW description of interface physics in 3D statistical models.

Acknowledgements

We are grateful to M. Caselle and F. Gliozzi for many useful suggestions. One of us (S.V.) would like to thank S. Alves Dias, M. G. do Amaral, C. A. Linhares, J. Mignaco and M. A. do Rego Monteiro for stimulating discussions and the CBPF for the kind and warm hospitality at Rio de Janeiro. The work of P.P. is supported by an INFN grant. The work of S.V. at Rio de Janeiro is supported by an CNPq grant.

Figure Captions

Fig. 1. *Hystogram of the real part of the magnetization for a typical MC ensemble (in this case $T = 20$, $R = 20$). The absence of a peak in Re $M = 0$ indicates that the disordered phase do not coexist with the ordered ones at our $\beta = 0.3680$.*

Fig. 2. *Distribution of a sample of 1,000 configurations generated by the MC simulation in the complex plane of the magnetization for a lattice $T = R = 20$. The three clusters of points represent the one-phase configurations; the straight lines joining the clusters are the two-interface configurations.*

Fig. 3. *The same of Fig. 2 for a lattice $T = 10$, $R = 20$. The three-interface configurations are uniformly distributed in the interior of the triangle.*

Fig. 4. *Comparison of the predictions of the CW model with the MC data E versus $z = R/T$. The lines represent the best fit of all data to formula (8): from up to down they correspond respectively to $R = 9, 10, 11$ fixed (cfr. Tab. 1).*

Fig. 5. *Comparison of the predictions of the classical formula model with the MC data E versus $A_m = RT$. The line represent the best fit of the symmetric $T = R$ data to formula (17); the asymmetric MC data are also reported (cfr. Tab. 1).*

Fig. 6. *Comparison of the predictions of the 2-loop (8) approximation and that of the 1-loop (18) for the $(R, T = 11)$ data, with $z = R/T$. The dashed line represent the 1-loop best fit while the 2-loop is the dotted line.*

fig.1

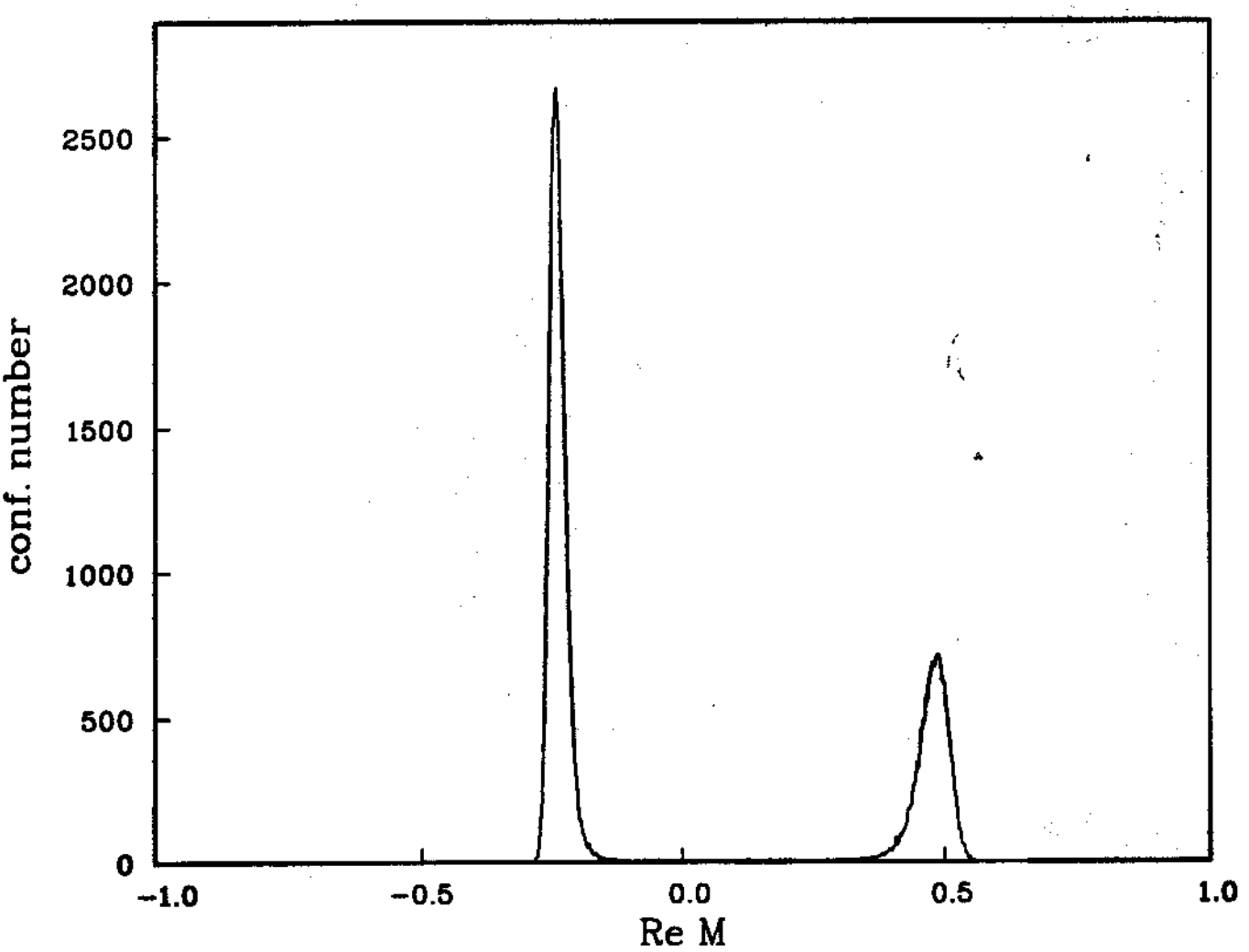

fig.2

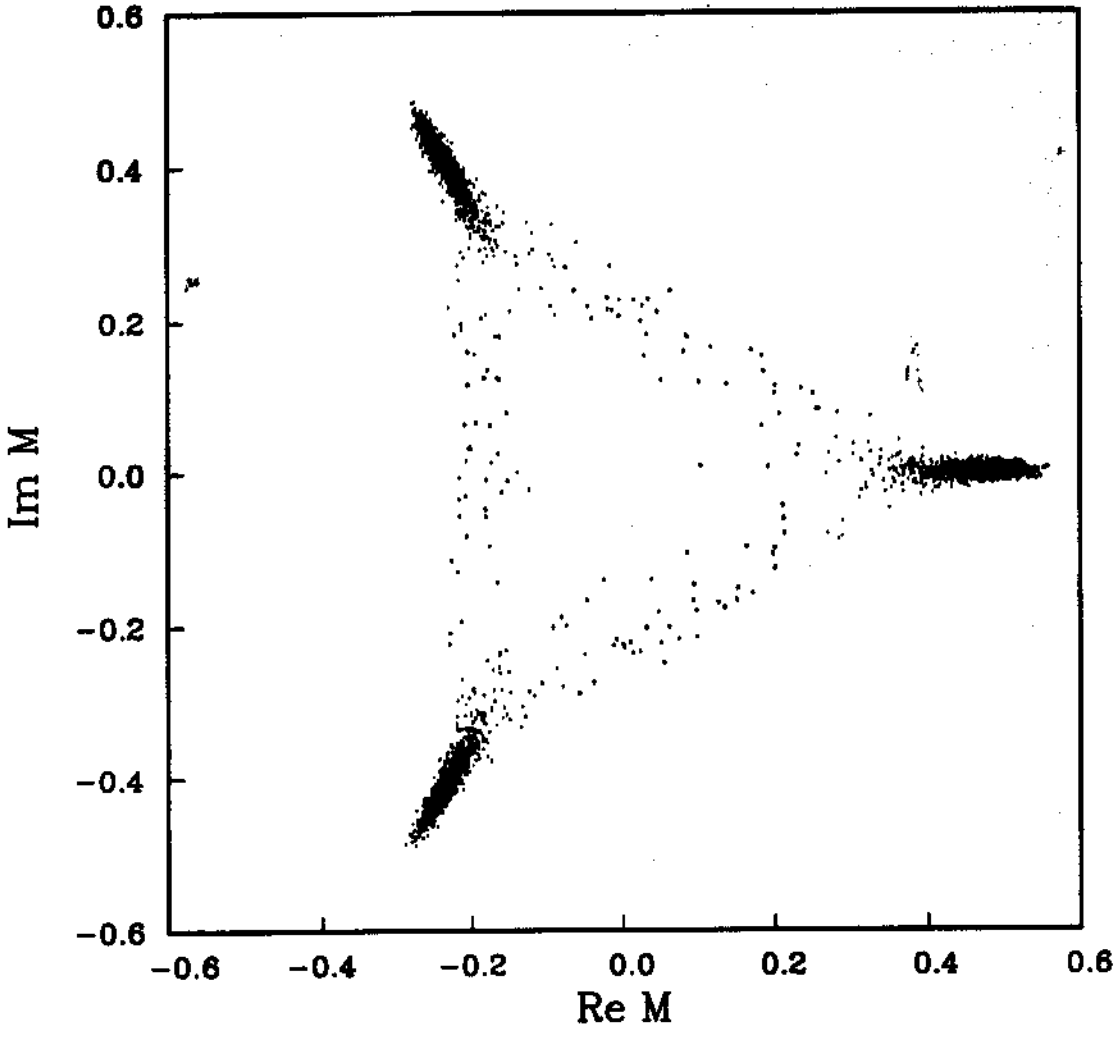

fig.3

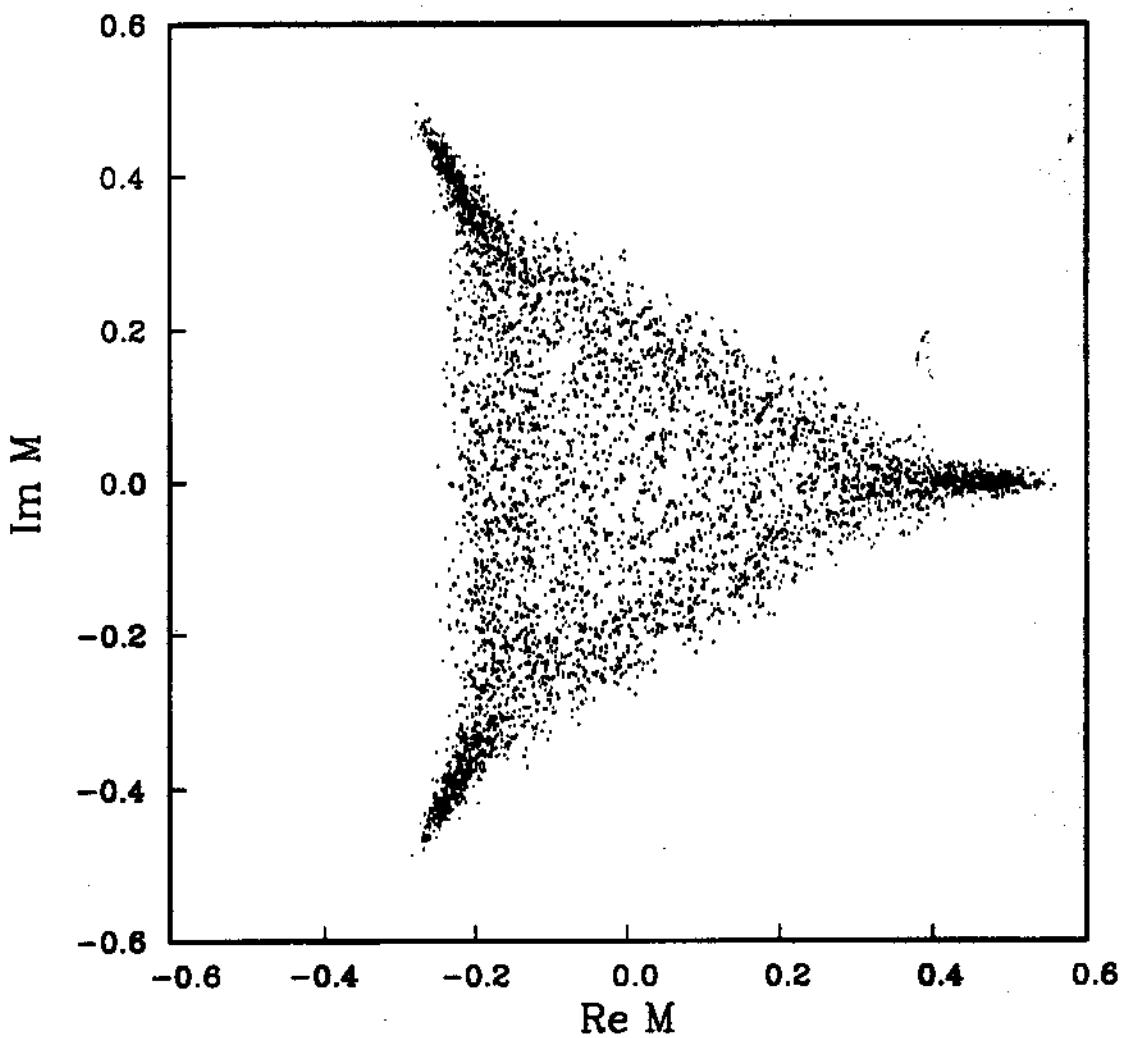

fig.4

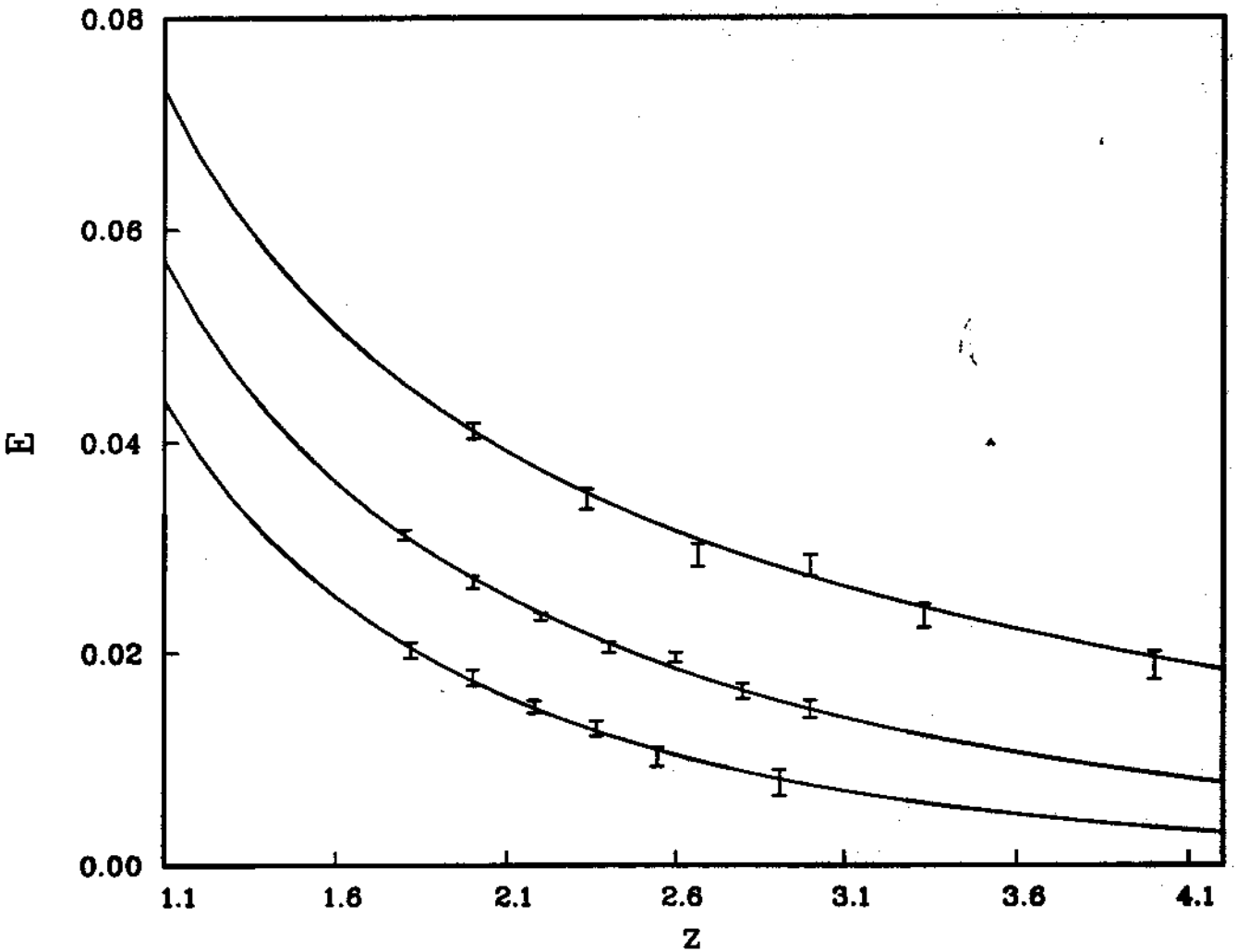

fig.5

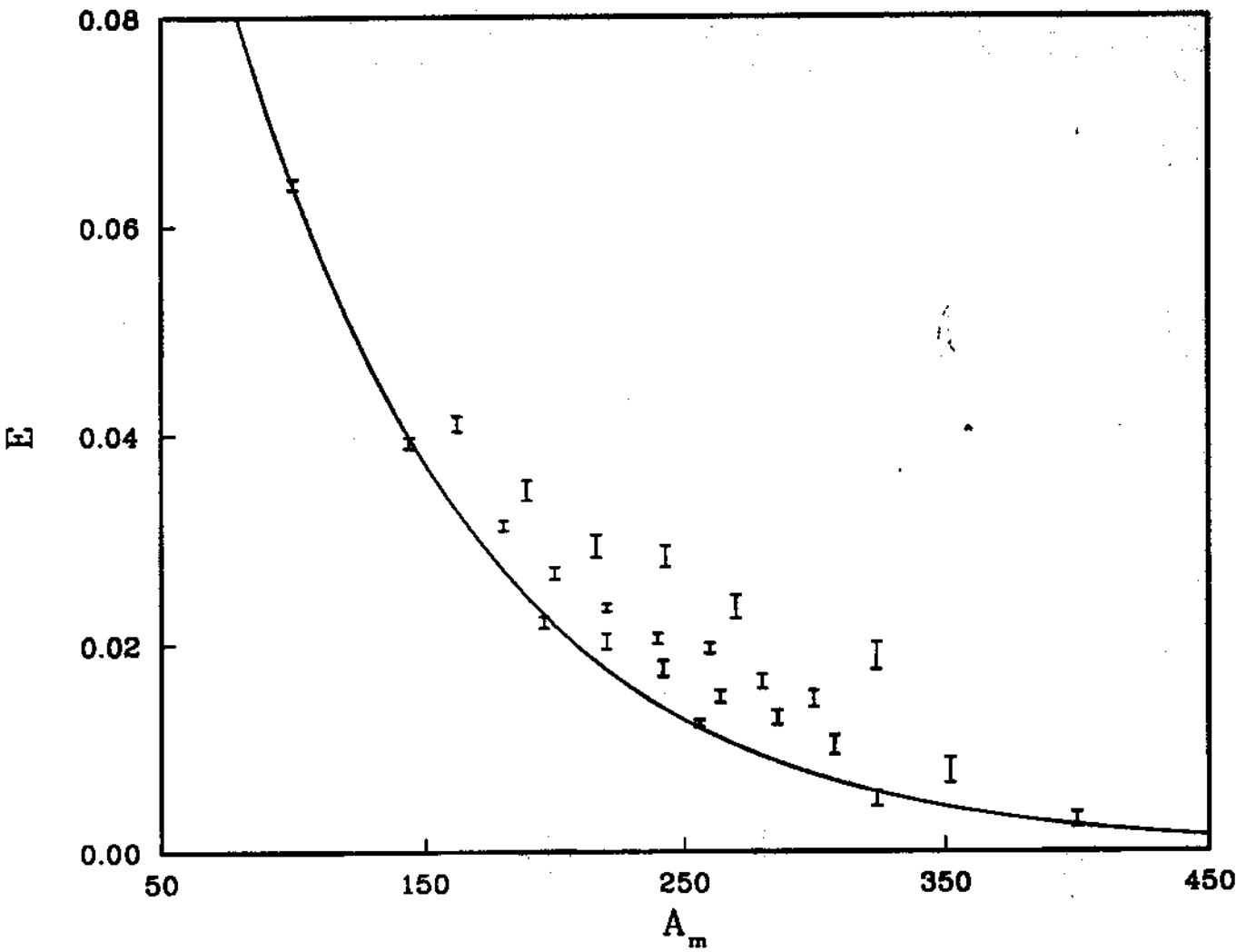

fig.6

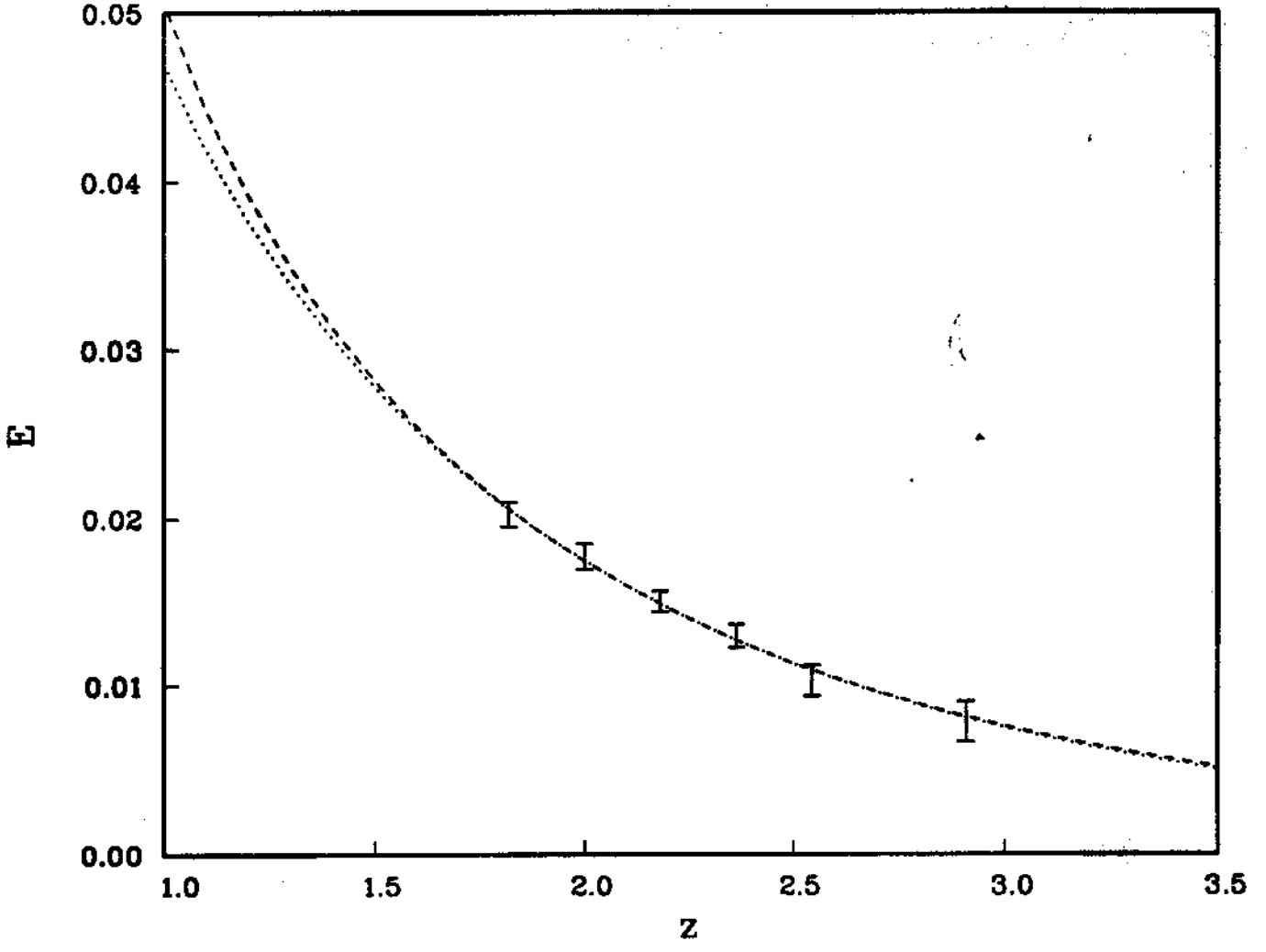

References

[1] M. P. Gelfand and M. E. Fisher, *Physica* **A 166** (1990) 1

[2] F. P. Buff, R. A. Lovett and F. H. Stillinger Jr., *Phys. Rev. Lett.* **15** (1965) 621

[3] M. Caselle, F. Gliozzi and S. Vinti, *Phys. Lett.* **B 302** (1993) 74

[4] C. Itzykson and J. B. Zuber, *Nucl. Phys.* **B 275**[FS17] (1986) 580

[5] B. Bunk, *Int. J. Mod. Phys.* **C 3** (1992) 889

[6] K. Dietz and T. Filk, *Phys. Rev.* **D 27** (1983) 2944

[7] R. V. Gavai, F. Karsh and B. Peterson, *Nucl. Phys.* **B 322** (1989) 738

[8] J. M. Drouffe and J. B. Zuber, *Phys. Rep.* **C 102** (1983) 1

[9] M. E. Fischer, *J. Phys. Soc. Japan Suppl.* **26** (1969) 87
M. E. Fischer and V. Privman, *J. Stat. Phys.* **33** (1983) 385
E. Brézin and J. Zinn-Justin, *Nucl. Phys.* **B 257**[FS14] (1985) 867
G. Münster, *Nucl. Phys.* **B 340** (1990) 559

[10] S. Klessinger and G. Münster, *Nucl. Phys.* **B 386** (1992) 701

[11] F. Karsch and A. Patkós, *Nucl. Phys.* **B 350** (1991) 563

[12] S. Gupta, A. Irbäck, B. Petersson, R. V. Gavai and F. Karsch, *Nucl. Phys.* **B 329** (1990) 263

[13] R. H. Swendsen and J. S. Wang, *Phys. Rev. Lett.* **58** (1987) 86

[14] Y. Iwasaki, K. Kanaya, Leo Käkkäinen, K. Rummukainen and T. Yoshié, *preprint CERN-TH.6798/93*, HEP-LAT 9309003, September 1993